



Contents lists available at ScienceDirect

Bioorganic & Medicinal Chemistry

journal homepage: www.elsevier.com/locate/bmc

Fluorescent analogs of peptoid-based HDAC inhibitors: Synthesis, biological activity and cellular uptake kinetics

Rick Raudszus^{a,b}, Robert Nowotny^c, Christoph G.W. Gertzen^{d,e}, Andrea Schöler^a, Andor Krizsan^{f,g}, Ines Gockel^c, Hermann Kalwa^b, Holger Gohlke^{d,e}, René Thieme^c, Finn K. Hansen^{a,*}

^a Pharmaceutical/Medicinal Chemistry, Institute of Pharmacy, Medical Faculty, Leipzig University, Brüderstraße 34, 04103 Leipzig, Germany

^b Rudolf Boehm Institute of Pharmacology and Toxicology, Medical Faculty, Leipzig University, Härtelstraße 16-18, 04107 Leipzig, Germany

^c Department of Visceral, Transplant, Thoracic and Vascular Surgery, University Hospital of Leipzig, Liebigstraße 20, 04103 Leipzig, Germany

^d Institute for Pharmaceutical and Medicinal Chemistry, Heinrich Heine University Düsseldorf, Universitätsstr. 1, 40225 Düsseldorf, Germany

^e John von Neumann Institute for Computing (NIC), Jülich Supercomputing Centre (JSC) and Institute for Complex Systems – Structural Biochemistry (ICS-6),

Forschungszentrum Jülich GmbH, Wilhelm-Johnen-Straße, 52428 Jülich, Germany

^f Institute of Bioanalytical Chemistry, Faculty of Chemistry and Mineralogy, Leipzig University, Deutscher Platz 5, 04103 Leipzig, Germany

^g Center for Biotechnology and Biomedicine, Leipzig University, Deutscher Platz 5, 04103 Leipzig, Germany

ARTICLE INFO

Keywords:

Cancer
Histone deacetylase
HDAC inhibitor
Peptoid
Fluorescent probes

ABSTRACT

Fluorescent tagging of bioactive molecules is a powerful tool to study cellular uptake kinetics and is considered as an attractive alternative to radioligands. In this study, we developed fluorescent histone deacetylase (HDAC) inhibitors and investigated their biological activity and cellular uptake kinetics. Our approach was to introduce a dansyl group as a fluorophore in the solvent-exposed cap region of the HDAC inhibitor pharmacophore model. Three novel fluorescent HDAC inhibitors were synthesized utilizing efficient submonomer protocols followed by the introduction of a hydroxamic acid or 2-aminoanilide moiety as zinc-binding group. All compounds were tested for their inhibition of selected HDAC isoforms, and docking studies were subsequently performed to rationalize the observed selectivity profiles. All HDAC inhibitors were further screened in proliferation assays in the esophageal adenocarcinoma cell lines OE33 and OE19. Compound **2**, 6-((N-(2-(benzylamino)-2-oxoethyl)-5-(dimethylamino)naphthalene)-1-sulfonamido)-N-hydroxyhexanamide, displayed the highest HDAC inhibitory capacity as well as the strongest anti-proliferative activity. Fluorescence microscopy studies revealed that compound **2** showed the fastest uptake kinetic and reached the highest absolute fluorescence intensity of all compounds. Hence, the rapid and increased cellular uptake of **2** might contribute to its potent anti-proliferative properties.

1. Introduction

Histone deacetylases (HDACs) catalyze the removal of acetyl groups of lysine side chains of histones and thereby play an important role in the regulation of transcription and protein expression.^{1,2} A dysregulated HDAC activity has been associated with cancer development and HDACs are often overexpressed in cancer cells.^{3,4} To date, 18 different HDAC isoforms were identified in the human genome and divided into four classes (I-IV). Only class I (HDACs 1, 2, 3 and 8), class IIa (HDACs 4, 5, 7, and 9) class IIb (HDACs 6 and 10), and class IV (HDAC 11) isoforms contain zinc-dependent catalytic domains, whereas class III isoforms (also called sirtuins) are NAD⁺-dependent enzymes.⁵ Although many effects of HDACs 1–3 are related to chromatin

remodeling, several non-histone proteins are also modulated by different HDAC isoforms.⁶ Comparing the 11 zinc-dependent isoforms in their localization, structure and substrates, HDAC6 is structurally and functionally unique. HDAC6 is the only isoform mainly located in the cytoplasm, is the only HDAC with two independent functional catalytic domains, and it is primarily acting via the deacetylation of non-histone substrates such as α -tubulin, cortactin or Hsp90.^{2,7,8}

HDACs are considered emerging epigenetic drug targets and four HDAC inhibitors (HDACi) have been approved by the U. S. Food and Drug Administration (FDA) to treat T-cell lymphoma or multiple myeloma (see Fig. 1).⁵ Furthermore, the class I selective aminoanilide-based HDACi tucidinostat (chidamide) was approved for the treatment of relapsed or refractory peripheral T-cell lymphoma (PTCL) in China.^{5,9}

* Corresponding author.

E-mail address: finn.hansen@uni-leipzig.de (F.K. Hansen).

<https://doi.org/10.1016/j.bmc.2019.07.055>

Received 26 March 2019; Received in revised form 23 July 2019; Accepted 31 July 2019

0968-0896/© 2019 Elsevier Ltd. All rights reserved.

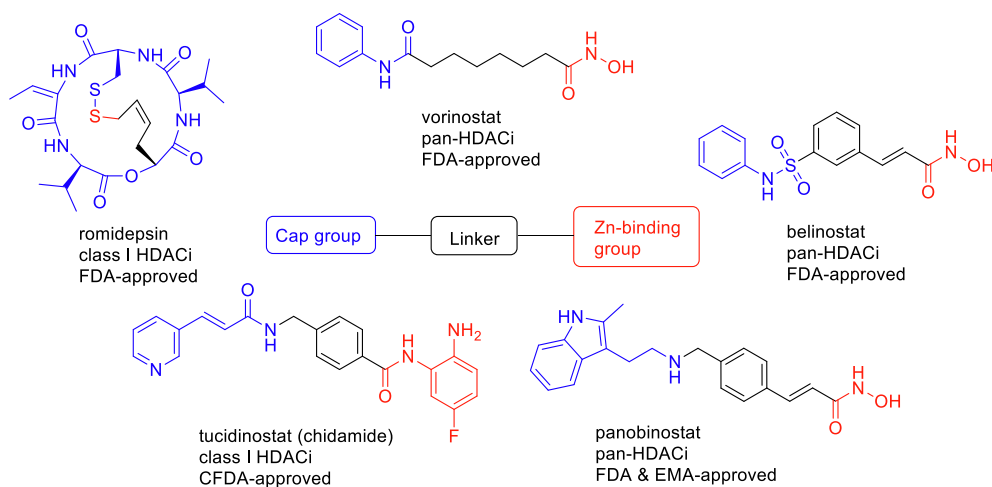


Fig. 1. Approved histone deacetylase inhibitors.

The molecular structure of HDACi can be described by a simple cap-linker-chelator pharmacophore model.⁵ The chelator or zinc-binding group (ZBG) chelates the catalytic zinc ion in the active site, the linker occupies the narrow hydrophobic tunnel inside the enzyme and the cap groups interacts with the surface area.¹⁰ First-generation HDACi are usually non-selective pan-inhibitors, which possess several side effects such as fatigue, diarrhea, weight loss, bone marrow depression, and cardiac arrhythmias.¹ Therefore, current drug discovery efforts focus on the development of class- or even isoform-preferential HDACi. The increasing number of available X-ray co-crystal structures has fueled the development of selective compounds and several class- and isoform-preferential HDACi are currently investigated in clinical trials.¹¹ However, there is still a lack of knowledge about the cellular penetration and subcellular location of different types of HDACi. Fluorescent tagging for cellular imaging and cell-based microscopy studies allow investigating subcellular localization and dynamics of drug targets.¹² Furthermore, fluorescent tagging represents a powerful alternative to radio-labelling to study cellular uptake kinetics. In this work, we describe the rational design, synthesis, biological activity and cellular uptake kinetics of a small series of novel fluorescent HDACi.

2. Results

2.1. Design and synthesis of target compounds

Peptoids (or *N*-substituted glycines) are peptidomimetic analogues of naturally occurring peptides. We have recently reported two types of peptoid-based HDACi that are easily accessible by a multi-component approach.^{13–16} Depending on the linker type and the nature of the cap group, the isoform preference can be altered from HDAC6 preferential to HDAC1-3 preferential.^{13–16} The aim of this work was to retain the *N*-substituted glycine (peptoid) scaffold and to introduce a fluorescent tag at the capping group, as this group is most solvent-exposed.

Accordingly, the HDACi pharmacophore model tolerates a variety of cap groups and this region has been used previously for labelling^{12,17,18} and hybridization^{19–21} approaches. The dansyl group is a widely used fluorophore and is structurally related to typical HDACi caps. For instance, both naphthyl and 4-dimethylaminophenyl residues were tolerated in our peptoid-based HDACi of type I and II.^{13,15,16} Therefore, the dansyl moiety was chosen as fluorescent tag in this study. Our design strategy included the variation of the linker and ZBG (Fig. 2). Compound 1 containing a benzyl linker was designed based on our HDAC6 preferential inhibitors of type I, whereas compound 2 is derived from our class I preferential peptoids of type II. The aminoanilide group (as realized in e.g. tucidinostat) is an alternative ZBG with class I selectivity and slow off binding kinetics.²² The well-established

class I selective HDACi tucidinostat, entinostat and mocetinostat are all utilizing a benzyl linker in combination with the aminoanilide ZBG. Thus, compound 3 was designed as a potential class I selective HDACi featuring a benzyl group as linker and an aminoanilide ZBG.

The target compounds 1–3 were synthesized as summarized in Schemes 1–3. In the first step benzylamine 4 was acylated with bromoacetyl bromide 5 to provide the bromoacetyl amide 6. Next, methyl 4-(aminomethyl)benzoate hydrochloride was reacted with 6 using triethylamine as base to afford the secondary amine 7. Subsequently, the fluorescent tag was introduced by the treatment of 7 with dansyl chloride. The synthesis of the target compound 1 was finally accomplished by the hydroxylaminolysis of the methyl ester derivative 8 (Scheme 1). The target compound 2 was synthesized using a similar synthetic pathway (Scheme 2). Briefly, the alkylation of methyl 6-aminohexanoate hydrochloride with 6 in the presence of triethylamine in DCM provided the alkyl-substituted secondary amine 9. The introduction of the fluorophore followed by hydroxylaminolysis yielded the target compound 2. The aminoanilide-based HDACi 3 was prepared as illustrated in Scheme 3. The saponification of the key intermediate 8 afforded carboxylic acid 11. Next, 11 was coupled with mono-Boc-protected phenylenediamine 12 using HATU as coupling agent to furnish the Boc-protected compound 13. Finally, the treatment of 13 with trifluoroacetic acid in dichloromethane provided the desired aminoanilide-based HDACi 3.

2.2. Inhibition of HDAC1, 2, 3 & 6, cytotoxicity and hyperacetylation of histone H3 in esophageal adenocarcinoma cells OE33 & OE19

All synthesized fluorescent tagged compounds (1–3) were screened in a biochemical assay for their inhibition of selected HDAC isoforms using ZMAL (Z-Lys(Ac)-AMC) as substrate and compared to the inhibition capacity of vorinostat. HDAC1-3 were chosen as a representative class I isoforms. HDAC6 was selected because it is the main target of the peptoid-based HDACi of type I. The results are presented in Table 1. Compound 1 bearing a benzyl linker showed potent activity against HDAC6 (IC₅₀: 0.132 μM) and reduced activity against HDAC1 (IC₅₀: 0.915 μM), HDAC2 (IC₅₀: 3.50 μM) and HDAC3 (IC₅₀: 1.02 μM). Compound 2 containing an alkyl linker displayed unselective HDAC inhibition with IC₅₀ values in the double-digit nanomolar range (HDAC1 IC₅₀: 0.034 μM; HDAC2 IC₅₀: 0.081 μM; HDAC3 IC₅₀: 0.087 μM; HDAC6 IC₅₀: 0.046 μM). As expected, the aminoanilide 3 was inactive against HDAC6 (IC₅₀: > 10 μM) and showed submicromolar inhibition of HDAC1 (IC₅₀: 0.676 μM) and HDAC2 (IC₅₀: 0.668 μM).

Subsequently, compounds 1–3 and vorinostat were used in proliferation assays in the esophageal adenocarcinoma cell lines OE33 and OE19 for 72 h (Table 1). The esophageal adenocarcinoma still has a

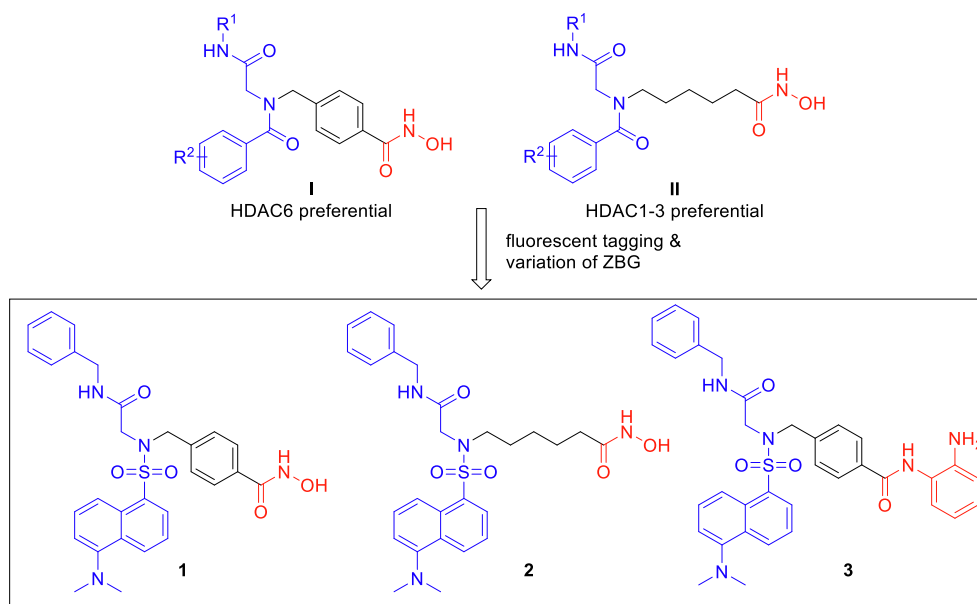


Fig. 2. Design of fluorescent analogs of peptoid-based HDAC inhibitors.

poor prognosis and only 50% of treated patients respond to chemotherapy. Therefore, novel concepts and treatment regimens, like HDACi, are needed to increase susceptibility to common chemotherapeutics and to improve patient outcome.²³ Compared with vorinostat (GI_{50} OE33: 1.12 μ M; GI_{50} OE19: 1.42 μ M) compounds **1** and **3** showed relatively high GI_{50} values and failed to inhibit the proliferation sufficiently in esophageal adenocarcinoma cells. However, HDACi **2** had an increased anti-proliferative activity with sub-micromolar GI_{50} values of 0.776 μ M (OE33) and 0.925 μ M (OE19). To confirm the HDAC inhibitory activity in vitro, histone H3 (Lys9) acetylation was analyzed by western blot analysis after HDACi treatment for 48 h (**1**: 6.5 μ M; **2**: 2.25 μ M; **3**: 0.6 μ M). All compounds induced histone H3 hyperacetylation in comparison to untreated controls in OE33 and OE19 cells, clearly demonstrating the inhibitory capacity of HDACi **1–3** in an in vitro cellular model. Representative western blots for OE33 and OE19 are shown in Fig. S1 (Supporting Information).

Taken together, the benzyl-based HDACi **1** revealed HDAC6 preferential inhibition, whereas compound **2** with an alkyl linker showed potent and unselective inhibition of HDAC1-3 and HDAC6 with IC_{50} values in the double-digit nanomolar concentration range. The aminoanilide **3** was identified as a moderate and preferential inhibitor of HDAC1-3. In agreement with the results from the biochemical assays, compound **2** displayed the highest anti-proliferative activity of all compounds and exceeded activity of the reference HDACi vorinostat.

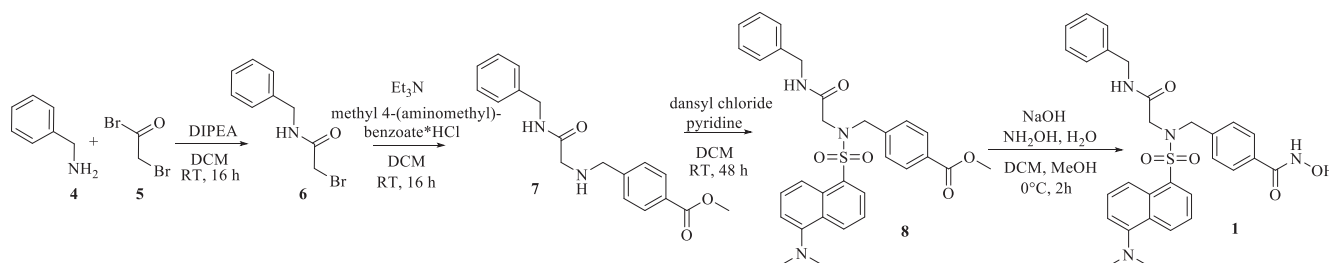
2.3. Molecular modelling and docking studies

In order to find a structural explanation for the selectivity profiles of the HDACi, compounds **1–3** were docked into the binding pockets of the

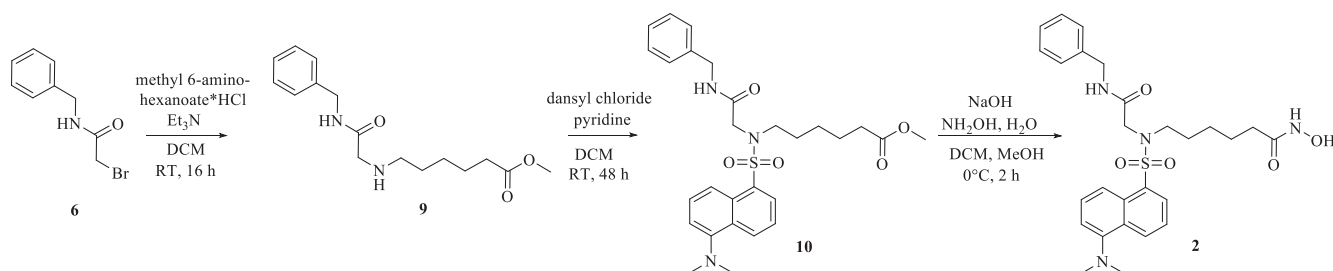
X-ray crystal structures of HDAC1 and HDAC6 as representatives for HDAC classes I and IIb, respectively. We identified binding poses of all compounds interacting with the zinc ions via their ZBG except for compound **3** in HDAC6 (Table 2), likely due to its spacious ZBG. This is in accordance with compound **3** being inactive towards HDAC6 (Table 1). For the remaining ligand-receptor combinations, the respective IC_{50} values roughly correlate with the size of the largest pose cluster, a proxy for how favorable the docking is.²⁴ As such, compound **2**, which exhibits the lowest IC_{50} towards all tested HDAC isoforms, always contains > 50% of all docking poses in that cluster, although it does not always show the lowest docking energy (Table 2). The binding poses of the three compounds in HDAC1 exhibit a similar orientation, with the benzyl moiety interacting with H28 and F150, while the dansyl moiety interacts with Y204 and L271 (Fig. 3A-C). As to differences among the HDACi, compound **2** binds to the zinc ion with optimal geometry (distance \approx 2.1 Å), and compound **1** cannot form π -stacking interactions with F205. Compound **3**, in turn, forms π -stacking interactions with F205 but shows an increased distance to the zinc ion by 1.4 Å compared to compound **2**. This could explain why compound **2** exhibits the lowest IC_{50} towards HDAC1. In HDAC6 compound **2** forms equally favorable contacts as in HDAC1, while the distance and binding geometry of the ZBG of compound **1** is more favorable in HDAC6 (Fig. 3C, D). Hence, our docking reproduces the selectivity profile of compounds **1–3**.

2.4. Photophysical data

In order to characterize the photophysical properties of the synthesized compounds, the absorption and emission spectra as well as the



Scheme 1. Synthesis of compound **1**.



Scheme 2. Synthesis of compound 2.

Stokes shift of the three fluorescent-tagged compounds (1–3) were determined in three different polar solvents (Table S1, Supporting Information). Water as solvent generated lower Stokes shifts (138–166 nm) because of the higher wavelengths of the absorption maxima and the lower wavelengths of the emission maxima.

The opposite was observed for methanol and DMSO, which resulted in higher Stokes shifts (186–202 nm).

2.5. Fluorescence microscopy und cellular uptake kinetics

Fluorescent tagging represents a simple and efficient method to study cell penetration of small molecules. Therefore, we utilized the fluorescent properties of our compounds 1–3 to monitor their cellular uptake by fluorescence microscopy. OE33 (Fig. 4A) and OE19 (Fig. 4B) cells were treated with 1–3 (1.25 μ M) for 30 min. We were able to monitor an uptake kinetic for all three inhibitors. After 30 min the absolute fluorescence intensity was higher for all three compounds in the OE19 cells than the OE33 cells. Interestingly, inhibitor 2 displayed in both cell lines the fastest uptake kinetic and reached the highest absolute fluorescence intensity. Representative images are shown after HDACi treatment for 15 min (Fig. 4C). HDACi 1 and 3 showed comparable uptake kinetics but displayed slower uptake ratios than 2. Notably, HDACi 2 showed the strongest anti-proliferative activity of all three compounds and exceeded the activity of the reference compound vorinostat (Table 1). Previously, it has been hypothesized that it might be beneficial to enhance the cytotoxicity of HDACi by the simultaneous inhibition of class I and IIb isoforms.^{25–27} Thus, the high activity of HDACi 2 in the proliferation assays is most probably related to its unselective inhibition of class I HDAC isoforms and HDAC6 (Table 1). However, the results from our fluorescence microscopy study indicate that the rapid and more complete cellular uptake of HDACi 2 might contribute to the increased anti-proliferative activity of this compound compared to its analogs 1 and 3.

Finally, in order to investigate possible differences in the cellular retention of the fluorescent probes 1–3, we performed confocal microscopy studies and observed predominantly cytoplasmic retention of all three compounds (Fig. 4D). This is in accordance with previously published results.^{17,18} Additionally, we noticed a similar distribution of

the fluorescence signal after HDACi treatment for 48 h (Fig. S2, Supporting Information).

3. Conclusion

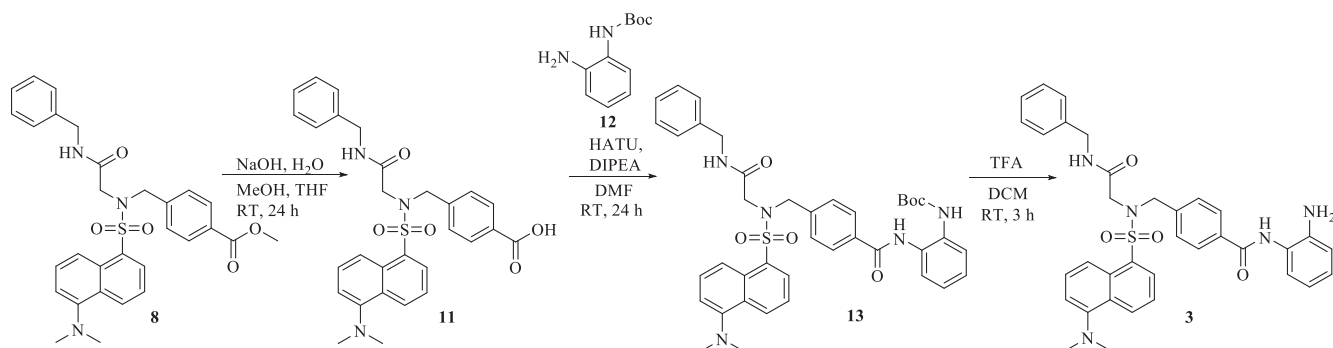
In summary, we have synthesized three novel HDACi with fluorescent properties and studied their biological activity and cellular uptake kinetics. The widely used dansyl group was chosen as the fluorescent tag and was introduced in the cap region of the HDACi pharmacophore model. The target compounds were synthesized using a straightforward submonomer protocol followed by the introduction of a hydroxamic acid or 2-aminoanilide function as ZBG. All three compounds were screened for their inhibition of recombinant HDAC1-3 and HDAC6. As expected, compound 1 with a benzyl linker displayed preferential inhibition of HDAC6, whereas the alkyl-based HDACi 2 showed potent and unselective inhibition of all tested isoforms with IC_{50} values in the double-digit nanomolar concentration range. The aminoanilide-based HDACi 3 revealed moderate and preferential inhibition of HDAC1-3. Molecular modelling and docking studies provided structural explanations for the observed differences in the HDAC isoform profiles of 1–3. Notably, compound 2 showed the highest anti-proliferative activity in proliferation assays with esophageal adenocarcinoma cells (OE33 and OE19) and exceeded the activity of the FDA-approved drug vorinostat. It can be assumed that this effect is related to its potent and unselective HDAC inhibitory activity. In addition, our results from a fluorescence microscopy study demonstrated differences in the cellular uptake of compounds 1–3. The rapid and increased cellular uptake of HDACi 2 might therefore contribute to its high anti-proliferative properties.

Taken together, our novel fluorescent HDACi 1–3 are promising starting points to study the uptake kinetics of HDACi into cancer cells and to investigate the subcellular location of histone deacetylases.

4. Experimental data

4.1. Chemistry

All reagents and solvents were commercially available and used



Scheme 3. Synthesis of compound 3.

Table 1
Inhibition of HDAC1, 2, 3 and 6 and inhibition of proliferation in the esophageal adenocarcinoma cells OE33 and OE19.

Compound	HDAC1 IC ₅₀ [μM]	HDAC2 IC ₅₀ [μM]	HDAC3 IC ₅₀ [μM]	HDAC6 IC ₅₀ [μM]	OE33 GI ₅₀ [μM]	OE19 GI ₅₀ [μM]
1	0.915 ± 0.006	3.50 ± 0.33	1.02 ± 0.13	0.132 ± 0.003	6.23 ± 0.91	12.9 ± 1.2
2	0.034 ± 0.001	0.081 ± 0.003	0.087 ± 0.008	0.046 ± 0.004	0.776 ± 0.195	0.925 ± 0.037
3	0.676 ± 0.130	0.668 ± 0.021	1.13 ± 0.006	> 10	4.59 ± 0.16	9.10 ± 0.72
Vorinostat	0.089 ± 0.001	0.183 ± 0.007	0.105 ± 0.004	0.038 ± 0.001	1.12 ± 0.35	1.42 ± 0.10

Table 2
Results of the docking of compounds 1–3 into the X-ray crystal structures of HDAC1 and HDAC6.

Compound	HDAC1 ¹	HDAC6 ¹
1	−11.61/20	−12.93/20
2	−15.22/55	−16.04/53
3	−17.77/29	n/a ²

¹ Docking energy in kcal mol^{−1}/percent of poses in largest cluster.

² No poses complexing the zinc ion were found.

without further purification. The high-resolution mass spectra were measured by the Leipzig University Mass Spectrometry Service using a Bruker Daltonics ESQUIRE 3000Plus (ESI). The nuclear magnetic resonance spectrometry was performed using Varian Mercury-300BB (300 MHz) or Varian Mercury-400BB (400 MHz) spectrometers. Chemical shifts (δ) are given in ppm relative to the residual signals of the respective solvents. ¹H NMR signals marked with an asterisk (*) correspond to peaks assigned to the major rotamer conformation. Coupling constants (J) are reported in hertz (Hz). Following types of signals were qualified: singlet (s), doublet (d), double doublet (dd), triplet (t), quartet (q) and multiplet (m). See [Supporting Information](#) for spectroscopic characterization. A Barnstead Electrothermal 9100 apparatus was used for the determination of melting points. Thin layer chromatography was carried out using Machery-Nagel precoated aluminum foil sheets. Vorinostat was synthesized according to the literature.²⁸ Analytical HPLC analysis were carried out on a HPLC system equipped with a Gynkotek Gina 50 (autosampler), Dionex P680 HPLC

(pumps), Gynkotek UVD 340U (UV-detector) using a Machery-Nagel EC 250/4 NUCLEODUR 100-5 C18ec column. UV absorption was detected at 254 nm with a linear gradient of 10% B to 95% B in 7 min followed by isocratic elution at 95% B for 10 min using HPLC-grade water + 0.1% TFA (solvent A) and HPLC-grade acetonitrile + 0.1% TFA (solvent B) for elution at a flow rate of 1 mL/min. The purity of all final compounds was 95% or higher.

4.1.1. N-Benzyl-2-bromoacetamide (6)

Benzylamine **4** (1.1 mL, 10 mmol, 1.0 eq) and DIPEA (1.7 mL, 10 mmol, 1.0 eq) were dissolved in dichloromethane (10 mL). Bromoacetyl bromide **5** (0.87 mL, 10 mmol, 1.0 eq) was added dropwise at 0 °C and the reaction was stirred for 16 h at room temperature. Afterwards the solvent was removed under reduced pressure. The remaining residue was suspended in 5% aqueous hydrochloric acid (5 mL) and extracted with dichloromethane (3 × 15 mL). The combined organic layers were dried over sodium sulfate and concentrated under reduced pressure to provide the bromoacetyl amide **6** as a yellow oil (2.27 g, 99%). ¹H NMR (400 MHz, CDCl₃) δ 7.41–7.31 (m, 5H), 6.79 (s, 1H), 4.51 (d, *J* = 5.7 Hz, 2H), 3.96 (s, 2H) ppm. ¹³C NMR (100 MHz, CDCl₃) δ 165.3, 137.2, 128.8, 127.8, 127.7, 44.2, 29.1 ppm. HRMS (ESI) *m/z* calculated for (M + Na)⁺ 249.984, found 249.9786.

4.1.2. Methyl 4-([2-(benzylamino)-2-oxoethyl]amino)methyl)benzoate (7)

Methyl 4-(aminomethyl)benzoate hydrochloride (2.0 g, 10 mmol, 1.0 eq) and triethylamine (2.8 mL, 20 mmol, 2.0 eq) were dissolved in dichloromethane (10 mL). After adding **6** (2.3 g, 10 mmol, 1.0 eq), the

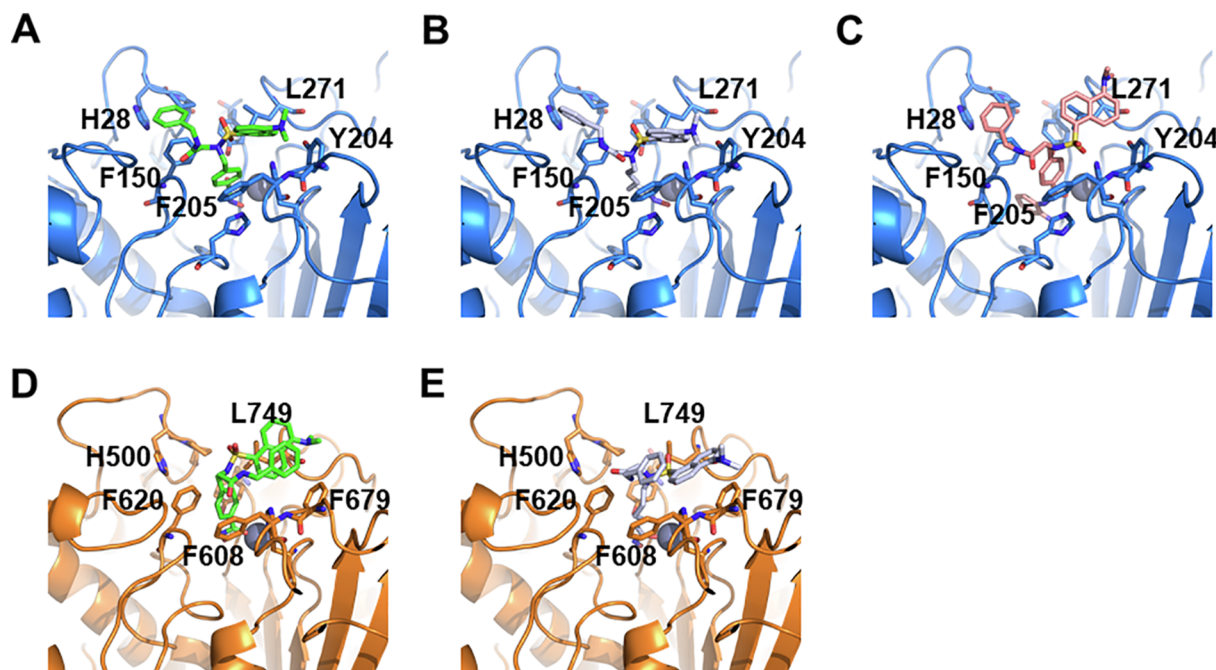


Fig. 3. Predicted binding poses of compounds 1 (A, D, green), 2 (B, E, gray), and 3 (C, salmon) in the X-ray crystal structures of HDAC1 (A-C, blue) and HDAC6 (D, E, orange). All three compounds complex the zinc ion (sphere) with their ZBGs.

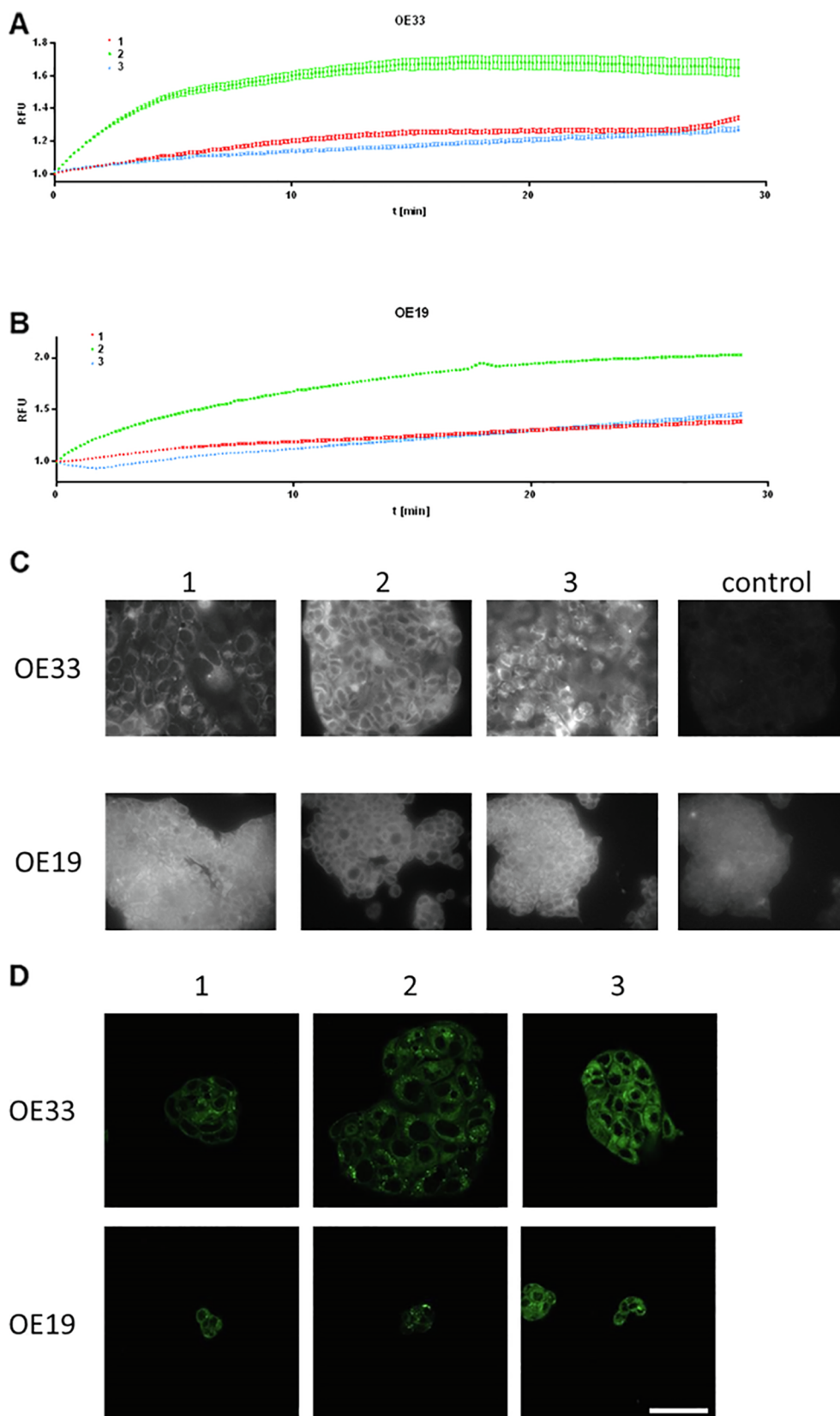


Fig. 4. Cellular uptake of compounds 1–3. A) OE33 and B) OE19 cells were treated with 1.25 μM of compound 1 (red), 2 (green) or 3 (blue) and the increase of the fluorescence intensity were measured ($E_{\text{ex}} = 370 \text{ nm}$ and $E_{\text{em}} = 530 \text{ nm}$) every 10 sec for 30 min. C) Representative pictures were shown for compound 1–3 and a control after 15 min. D) Confocal microscopy studies of OE33 and OE19 (50 μm scale) after 30 min incubation with compounds 1–3 (1.25 μM).

reaction was stirred for 16 h at room temperature after which the solvent was removed under reduced pressure. The remaining residue was suspended in water and the aqueous solution was extracted with dichloromethane (3 × 15 mL). The combined organic layers were washed with sodium bicarbonate solution (3 × 10 mL) and brine (1 × 10 mL) dried over sodium sulfate and concentrated under reduced pressure. The crude product was purified by column chromatography (petroleum ether/ethyl acetate 75:25 to 0:100) to yield **7** as a yellow oil (2.2 g, 71%). ¹H NMR (400 MHz, CDCl₃) δ 8.00–7.95 (2-d, *J* = 8.2 Hz, 2H), 7.46–7.29 (m, 7H), 6.95 (s, 1H), 5.32 (s, 1H), 4.49*/4.44 (2-d, *J* = 5.8/5.9 Hz, 2H), 3.94 (s, 3H), 3.85*/3.81 (2-s, 2H), 3.39*/3.29 (2-s, 2H) ppm. ¹³C NMR (100 MHz, CDCl₃) δ 171.0, 166.8, 144.4, 138.1, 129.9, 129.3, 128.7, 127.9, 127.7, 127.5, 58.3, 53.6, 52.0, 43.0 ppm. HRMS (ESI) *m/z* calculated for (M + H)⁺ 313.1547, found 313.1504.

4.1.3. Methyl 6-([2-(benzylamino)-2-oxoethyl]amino)hexanoate (**9**)

Methyl 6-aminohexanoate hydrochloride (1.5 g, 8.0 mmol, 1.0 eq) and triethylamine (2.2 mL, 16 mmol, 2.0 eq) were dissolved in dichloromethane (10 mL). Next, **6** (1.8 g, 8.0 mmol, 1.0 eq) was added and the mixture was stirred for 16 h at room temperature. The solvent was removed under reduced pressure and the crude product was purified by column chromatography (DCM/MeOH 100:0 to 90:10) to yield **9** as a yellow oil (0.75 g, 32%): ¹H NMR (400 MHz, CDCl₃) δ 7.65 (s, 1H), 7.38–7.29 (m, 5H), 7.27 (s, 1H), 4.49 (d, *J* = 5.9 Hz, 2H), 3.67 (s, 3H), 3.35 (s, 2H), 2.62 (m, 2H), 2.29 (m, 2H), 1.60 (m, 2H), 1.48 (m, 2H), 1.34 (m, 2H) ppm. ¹³C NMR (75 MHz, CDCl₃) δ 173.9, 171.3, 138.4, 128.6, 127.6, 127.3, 52.4, 51.5, 49.8, 42.9, 33.8, 29.5, 26.5, 24.5 ppm. HRMS (ESI) *m/z* calculated for (M + H)⁺ 293.1860, found 293.1720.

4.1.4. Methyl 4-([N-[2-(benzylamino)-2-oxoethyl]-5-(dimethyl-amino)naphthalene]-1-sulfonamido)-methyl]benzoate (**8**)

Compound **7** (0.31 g, 1.0 mmol, 1.0 eq) was dissolved in dichloromethane (15 mL) and the reaction was cooled down to 0 °C before first pyridine (89 μL, 1.1 mmol, 1.1 eq) and second dansyl chloride (0.30 g, 1.1 mmol, 1.1 eq) were added consecutively. The reaction was stirred at room temperature for 48 h. Afterwards the solvent was removed under reduced pressure and the residue was suspended in water. The aqueous solution was extracted with dichloromethane (3 × 15 mL), washed with saturated sodium bicarbonate solution (10 mL), 2% aqueous hydrochloric acid (10 mL) and brine (10 mL). The organic phase was dried over sodium sulfate and the solvent was removed under reduced pressure. Finally, the residue was purified by column chromatography (petroleum ether/ethyl acetate 75:25 to 0:100) which yielded the ester **8** as a yellow solid (0.28 g, 52%). Mp 89–90 °C; ¹H NMR (400 MHz, CDCl₃) δ 8.62 (d, *J* = 8.5 Hz, 1H), 8.33–8.27 (m, 2H), 7.88 (d, *J* = 8.0 Hz, 2H), 7.55 (q, *J* = 8.3 Hz, 2H), 7.33–7.30 (m, 1H), 7.27–7.18 (m, 4H), 7.05–7.00 (m, 2H), 6.49–6.41 (m, 1H), 5.32 (s, 1H), 4.58 (s, 2H), 4.12 (d, *J* = 5.7 Hz, 2H), 3.94 (s, 3H), 3.89 (s, 2H), 2.93 (s, 6H) ppm. ¹³C NMR (100 MHz, CDCl₃) δ 167.4, 166.4, 152.1, 139.6, 137.2, 132.9, 131.4, 130.7, 130.1, 130.1, 129.8, 128.9, 128.8, 128.6, 127.5, 127.4, 126.4, 123.2, 118.4, 115.4, 52.8, 52.1, 50.8, 45.3, 43.3 ppm. HRMS (ESI) *m/z* calculated for (M + H)⁺ 546.1984, found 546.1946.

4.1.5. Methyl 6-([N-[2-(benzylamino)-2-oxoethyl]-5-(dimethyl-amino)naphthalene]-1-sulfonamido)hexanoate (**10**)

Compound **9** (0.75 g, 2.6 mmol, 1.0 eq) was dissolved in dichloromethane (20 mL) and the mixture was cooled down to 0 °C before first pyridine (0.23 mL, 2.8 mmol, 1.1 eq) and second dansyl chloride (0.76 g, 2.8 mmol, 1.1 eq) were added consecutively. The reaction was stirred at room temperature for 48 h. The solvent was removed under reduced pressure and the residue was purified as described in 4.1.4 to yield the ester **10** as a yellow oil (0.96 g, 71%). ¹H NMR (400 MHz, CDCl₃) δ 8.70 (s, 1H), 8.34 (s, 1H), 8.22 (d, *J* = 7.2 Hz, 1H), 7.63–7.52 (m, 2H) 7.36–7.30 (m, 3H), 7.18 (d, *J* = 8.0 Hz, 2H), 6.88–6.83 (m,

1H), 5.33 (s, 1H), 4.35 (d, *J* = 5.7 Hz, 2H), 3.90 (s, 2H), 3.69 (s, 3H); 3.34 (t, *J* = 8.0 Hz, 2H), 2.97 (s, 6H), 2.19 (t, *J* = 7.4 Hz, 2H), 1.54–1.46 (m, 4H), 1.24–1.14 (m, 2H) ppm. ¹³C NMR (100 MHz, CDCl₃) δ 173.7, 168.3, 137.5, 133.1, 131.1, 130.4, 130.0, 129.9, 129.8, 128.7, 128.6, 127.6, 127.5, 123.3, 118.6, 115.4, 51.5, 51.4, 49.7, 45.4, 43.4, 33.6, 27.7, 26.1, 24.2 ppm. HRMS (ESI) *m/z* calculated for (M – H)[–] 524.2225, found 524.2385.

4.1.6. 4-([N-[2-(Benzylamino)-2-oxoethyl]-5-(dimethylamino)naphthalene]-1-sulfonamido)methyl-N-hydroxybenzamide (**1**)

Sodium hydroxide (88 mg, 2.2 mmol, 10 eq) and hydroxylamine 50% aqueous (0.40 mL, 6.6 mmol, 30 eq) were dissolved in methanol (3 mL) and dichloromethane (1 mL). Then, ester **8** (0.12 g, 0.22 mmol, 1.0 eq) was added and the reaction was stirred at 0 °C for 2 h. The reaction was monitored by thin layer chromatography. Upon completion, the solvents were removed under reduced pressure. The solid residue was suspended in water (1 mL) and the pH was adjusted to 7–8 using 10% aqueous hydrochloric acid. The precipitate was isolated by filtration and washed with cold water and cold diethyl ether to yield hydroxamic acid **1** as a yellow solid (0.11 g, 93%). Mp 127 °C; ¹H NMR (300 MHz, DMSO-*d*₆) δ 9.03 (s, 1H), 8.47 (d, *J* = 8.5 Hz, 1H), 8.34–8.26 (m, 2H), 8.22 (d, *J* = 8.6 Hz, 1H), 7.63–7.53 (m, 4H), 7.32–7.16 (m, 5H), 7.15–7.07 (m, 4H), 4.61 (s, 2H), 4.13 (d, *J* = 5.8 Hz, 2H), 3.93 (s, 2H), 2.82 (s, 6H) ppm. ¹³C NMR (75 MHz, DMSO-*d*₆) δ 208.5, 167.5, 163.9, 151.8, 139.3, 139.0, 135.8, 132.7, 130.3, 129.8, 129.6, 129.3, 128.6, 128.5, 127.7, 127.6, 127.2, 124.0, 119.3, 115.6, 51.3, 48.4, 45.5, 42.4 ppm. HRMS (ESI) *m/z* calculated for (M – H)[–] 545.1864, found 545.2056.

4.1.7. 6-([N-[2-(Benzylamino)-2-oxoethyl]-5-(dimethyl-amino)naphthalene]-1-sulfonamido)-N-hydroxyhexanamide (**2**)

Sodium hydroxide (0.19 g, 4.8 mmol, 10 eq) and hydroxylamine 50% aqueous (0.88 mL, 14 mmol, 30 eq) were dissolved in methanol (3 mL) and dichloromethane (1 mL). Then, ester **10** (0.25 g, 0.48 mmol, 1.0 eq) was added and the reaction was stirred at 0 °C for 2 h. The reaction was monitored by thin layer chromatography. Upon completion, the solvents were removed under reduced pressure. The solid residue was suspended in water (1 mL) and the pH was adjusted to 7–8 using 10% aqueous hydrochloric acid. The precipitate was isolated by filtration and washed with cold water and cold diethyl ether to yield hydroxamic acid **2** as yellow powder (0.21 g, 85%). Mp 84 °C; ¹H NMR (400 MHz, DMSO-*d*₆) δ 9.42 (s, 1H), 8.55 (s, 1H), 8.44 (d, *J* = 8.8 Hz, 1H), 8.21–8.16 (m, 2H), 7.61–7.54 (m, 2H), 7.32–7.14 (m, 7H), 4.22 (s, 2H), 4.02 (s, 2H), 3.28–3.24 (m, 2H), 2.80 (s, 6H), 1.74 (t, *J* = 7.4 Hz, 2H), 1.42–1.34 (m, 2H), 1.32–1.24 (m, 2H), 1.04–0.96 (m, 2H) ppm. ¹³C NMR (100 MHz, DMSO-*d*₆) δ 168.8, 168.1, 151.7, 139.5, 136.0, 130.0, 129.8, 129.6, 128.7, 128.6, 128.4, 127.6, 127.2, 124.0, 119.4, 115.5, 49.1, 48.4, 45.5, 42.5, 32.8, 27.3, 26.1, 25.3 ppm. HRMS (ESI) *m/z* calculated for (M – H)[–] 525.2177, found 525.2264.

4.1.8. 4-([N-[2-(Benzylamino)-2-oxoethyl]-5-(dimethylamino)naphthalene]-1-sulfonamido)methylbenzoic acid (**11**)

To a solution of sodium hydroxide (62 mg, 1.5 mmol, 4.0 eq) in water (0.5 mL), methanol (0.5 mL) and tetrahydrofuran (4 mL) was added ester **8** (0.21 g, 0.39 mmol, 1.0 eq) and the reaction was stirred at room temperature for 24 h. The solvents were removed under reduced pressure and the solid residue was dissolved in a sodium bicarbonate solution (15 mL). After extraction of the aqueous solution with ethyl acetate (3 × 15 mL) the pH of the aqueous phase was adjusted to 5 using 10% aqueous hydrochloric acid. The aqueous phase was extracted with ethyl acetate (3 × 15 mL) and the combined organic layers were washed with brine and dried over sodium sulfate. Removing the solvent under reduced pressure provided the carboxylic acid **11** as a yellow solid (0.19 g, 94%). Mp 130–131 °C; ¹H NMR (400 MHz, DMSO-*d*₆) δ 12.94 (s, 1H), 8.48 (d, *J* = 8.5 Hz, 1H), 8.35–8.32 (m, 2H), 8.24 (d, *J* = 8.6 Hz, 1H), 7.77 (d, *J* = 8.2 Hz, 2H), 7.60 (t, *J* = 8.0 Hz, 2H),

7.30–7.26 (m, 3H), 7.24–7.20 (m, 3H), 7.14–7.11 (m, 2H), 4.67 (s, 2H), 4.16 (d, $J = 5.8$ Hz, 2H), 3.99 (s, 2H), 2.84 (s, 6H) ppm. ^{13}C NMR (100 MHz, DMSO- d_6) δ 167.5, 167.4, 151.8, 142.2, 139.2, 135.8, 130.4, 130.3, 129.8, 129.7, 129.5, 129.3, 128.7, 128.6, 128.5, 127.6, 127.2, 124.0, 119.3, 115.6, 51.4, 48.7, 45.5, 42.4 ppm. HRMS (ESI) m/z calculated for $(\text{M}-\text{H})^-$ 530.1755, found 530.1885.

4.1.9. *tert*-Butyl (2-{4-[(*N*-[2-(benzylamino)-2-oxoethyl]-5-(*di*-methylamino)naphthalene]-1-sulfonamido)methyl]benzamido}-phenyl)carbamate (**13**)

The carboxylic acid **11** (0.35 g, 0.65 mmol, 1.0 eq), *tert*-butyl(2-aminophenyl) carbamate **12** (0.14 g, 0.65 mmol, 1.0 eq) and HATU (0.25 g, 0.65 mmol, 1.0 eq) were dissolved in *N,N*-dimethylformamide (5 mL) and DIPEA (0.11 mL, 0.65 mmol, 1.0 eq) was added. The reaction was stirred at room temperature for 24 h after which the solvent was removed under reduced pressure. The residue was dissolved in dichloromethane (20 mL). After washing with 1% aqueous hydrochloric acid (3×15 mL), saturated aqueous sodium bicarbonate solution (3×15 mL) and brine (15 mL), the organic phase was dried over sodium sulfate. The solvent was removed under reduced pressure to yield compound **13** as a brown solid (0.43 mg, 92%). Mp 93 °C; ^1H NMR (300 MHz, CDCl_3) δ 9.16 (s, 1H), 8.63 (d, $J = 8.5$ Hz, 1H), 8.32 (d, $J = 8.7$ Hz, 1H), 8.27 (dd, $J = 7.4$ Hz, 1.2 Hz, 1H), 7.78 (d, $J = 8.0$ Hz, 3H), 7.53 (q, $J = 8.2$ Hz, 2H), 7.32–7.27 (m, 2H), 7.25–7.13 (m, 7H), 7.01 (d, $J = 6.0$ Hz, 2H), 6.89 (s, 1H), 6.47 (t, $J = 5.9$ Hz, 1H), 4.57 (s, 2H), 4.12 (d, $J = 5.6$ Hz, 2H), 3.87 (s, 2H), 2.92 (s, 6H), 1.50 (s, 9H) ppm. ^{13}C NMR (100 MHz, CDCl_3) δ 167.4, 164.9, 154.6, 138.5, 137.3, 134.1, 133.2, 131.3, 130.7, 130.6, 130.0, 129.8, 129.1, 128.8, 128.6, 127.8, 127.5, 126.0, 125.9, 125.7, 124.5, 123.4, 115.6, 81.4, 52.6, 50.6, 45.4, 43.3, 38.6, 28.3, 22.6 ppm. HRMS (ESI) m/z calculated for $(\text{M}-\text{H})^-$ 720.2861, found 720.2957.

4.1.10. *N*-(2-Aminophenyl)-4-[(*N*-[2-(benzylamino)-2-oxoethyl]-5-(*dimethylamino*)naphthalene]-1-sulfonamido)methyl]benzamide (**3**)

Compound **13** (0.36 g, 0.50 mmol, 1.0 eq) was dissolved in dichloromethane (2.5 mL). Subsequently, trifluoroacetic acid (1.0 mL, 13 mmol, 26 eq) was added dropwise and the reaction was stirred at room temperature for 3 h. To stop the reaction, the pH was adjusted to 9 using sodium carbonate solution. Then, water (5 mL) was added to dilute the aqueous phase. Extraction with dichloromethane (3×15 mL), drying over sodium sulfate and removing the solvent under reduced pressure provided the aminoanilide **3** as a brown solid (0.27 g, 87%). Mp 116–117 °C; ^1H NMR (400 MHz, CDCl_3) δ 8.61 (d, $J = 8.5$ Hz, 1H), 8.34–8.28 (m, 2H), 7.76 (d, $J = 7.9$ Hz, 2H), 7.55 (q, $J = 7.6$ Hz, 3H), 7.40–7.30 (m, 4H), 7.27–7.18 (m, 4H), 7.14–7.08 (m, 2H), 7.04 (d, $J = 6.0$ Hz, 2H), 6.97–6.89 (m, 2H), 6.58–6.53 (m, 1H), 4.59 (s, 2H), 4.13 (d, $J = 5.8$ Hz, 2H), 3.86 (s, 2H), 2.93 (s, 6H) ppm. ^{13}C NMR (100 MHz, CDCl_3) δ 167.5, 165.2, 152.2, 140.4, 138.6, 137.3, 134.0, 133.1, 131.4, 130.7, 130.0, 129.8, 129.3, 128.9, 128.6, 127.8, 127.6, 127.5, 127.3, 125.2, 124.5, 123.3, 119.8, 118.5, 118.4, 115.5, 52.5, 50.4, 45.4, 43.3 ppm. HRMS (ESI) m/z calculated for $(\text{M} + \text{H})^+$ 622.2488, found 622.2624.

4.2. HDAC inhibition assays

The *in vitro* inhibitory activity of compounds **1–3** and vorinostat against human HDAC1, HDAC2, HDAC3/NcoR2 and HDAC6 were measured using a previously published protocol.²⁹ OptiPlate-96 black microplates (Perkin Elmer) were used with an assay volume of 50 μL . 5.0 μL test compound or control, diluted in assay buffer (50 mM Tris-HCl, pH 8.0, 137 mM NaCl, 2.7 mM KCl, 1.0 mM MgCl_2 , 0.1 mg/mL BSA), were incubated with 35 μL of the fluorogenic substrate ZMAL (Z-Lys(Ac)-AMC)³⁰ (21.43 μM in assay buffer) and 10 μL of human recombinant HDAC1 (BPS Bioscience, Catalog# 50051), HDAC2 (BPS Bioscience, Catalog# 50052), HDAC3/NcoR2 (BPS Bioscience, Catalog# 50003) or HDAC6 (BPS Bioscience, Catalog# 50006) at 37 °C. After an incubation time of 90 min, 50 μL of 0.4 mg/mL trypsin in

trypsin buffer (50 mM Tris-HCl, pH 8.0, 100 mM NaCl) were added, followed by further incubation at 37 °C for 30 min. Fluorescence was measured with an excitation wavelength of 355 nm and an emission wavelength of 460 nm using a Fluoroskan Ascent microplate reader (Thermo Scientific). All compounds were evaluated in duplicate in at least two independent experiments.

4.3. Photophysical data

For the absorption and emission spectra the compounds **1–3** were dissolved in water, methanol and DMSO each to get 1 M stock solutions. These stocks were diluted 1:10 three times and 200 μL of each dilution step plus blank were pipetted in a black 96-well plate. The absorption spectra (250 nm to 750 nm) and the emission spectra (400 nm to 650 nm) were measured in 2 nm steps using a SpectraMax Gemini EM Microplate Reader. The emission was stimulated by a wavelength near the absorption maximum.

4.4. Cell culture

The esophageal adenocarcinoma cells OE33 (ECACC-96070808) and OE19 (ECACC-96071721) were purchased from Sigma-Aldrich (Taufkirchen, Germany) and grown as described previously.³¹ For proliferation assays 3500 cells were seeded to 96-well plates and grown for 24 h before treated with either vorinostat or HDACi **1–3** for 72 h. Cells were incubated with PrestoBlue Cell Viability Reagent (ThermoFisher, Darmstadt, Germany) accordingly to the manufacturer's protocol.

Western blot analysis were performed as previously described.³² Briefly, 500,000 OE33 and 750,000 OE19 cells were seeded to 6-well plates and treated by HDACi **1–3** for 48 h. Cells were harvested, lysed and histones were isolated.³³ 5 μg of nuclear extract were separated on 15% sodium dodecyl sulphate (SDS)-polyacrylamide gels and blotted. Afterwards the membrane was blocked by 5% low fat milk/TBST for 1 h, incubated with a specific antibody against acetyl-histone H3 (Lys9) (#9649, CellSignaling, Danvers, USA) and histone H3 (#4499, Cell-Signalling, Danvers, USA) over night at 4 °C. A peroxidase coupled goat-anti-rabbit antibody (111-035-045, Jackson Immuno Research, Suffolk, UK) was used for the detection (1 h at room temperature) and visualized by ECL chemiluminescence (Millipore, Billerica, USA).

For the HDACi uptake kinetics, 500,000 cells were seeded to glass cover slips in 6-well plates and grown for 48 h. The analyses were done by HDACi treatment for 1 min and afterwards the fluorescence intensity was recorded by $E_{\text{ex}} = 370$ nm and $E_{\text{em}} = 530$ nm every 10 sec for 30 min using a Till Photonics Polychrome IV and a Zeiss Axiovert 100 equipped with a 40 \times Fluor 1.30.

For confocal microscopy studies, cells were treated as mentioned before. Additionally, cells were transfected with cDNA coding for histone H2b fused to the red fluorescent protein (H2B-RFP) with Fugene (Promega) according to the manufacturers protocol with a DNA to reagent ratio 1:1. Imaging experiments were performed with a Leica SP8 microscope using the lasX software package in combination with a 63 \times magnification lens and a 405 nm laser for excitation.

4.5. Molecular docking

For the molecular docking, compounds **1–3** were drawn and converted into a 3D structure with Maestro,³⁴ and energy-minimized with Moloc.^{35,36} The HDACi were then docked into crystal structures of HDAC1 (PDB ID: 4BKX³⁷) and HDAC6 (PDB ID: 5EDU⁷) utilizing AutoDock3^{38,39} as a docking engine and the DrugScore2018⁴⁰ distance-dependent pair-potentials as an objective function. In the docking, default parameters were used, with the exception of the clustering RMSD cutoff, which was set to 2.0 Å, to consider the flexibly connected saturated and unsaturated carbon cycles, as done previously.^{13,16,25} Docking solutions with more than 20% of all configurations in the

largest cluster were considered sufficiently converged.^{13,16,25} The configuration in the largest cluster with the lowest docking energy and with a distance < 3 Å between the hydroxamic acid oxygen and the zinc ion in the binding pocket was used for further evaluation.

Acknowledgements

We thank Prof. Dr. Ralf Hoffmann (Leipzig University) for providing us access to the SpectraMax Gemini EM Microplate Reader. We are grateful to the John von Neumann Institute for Computing (NIC) and the Jülich Supercomputing Centre for computing time on the supercomputer JURECA (NIC project HKF7 to H.G.). The authors would like to thank Franziska Rolfs for her excellent technical support.

Appendix A. Supplementary data

Supplementary data to this article can be found online at <https://doi.org/10.1016/j.bmc.2019.07.055>.

References

- Witt O, Deubzer HE, Milde T, Oehme I. HDAC family: what are the cancer relevant targets? *Cancer Lett.* 2009;277:8–21.
- Roche J, Bertrand P. Inside HDACs with more selective HDAC inhibitors. *Eur J Med Chem.* 2016;121:451–483.
- Mottamal M, Zheng S, Huang T, Wang G. Histone deacetylase inhibitors in clinical studies as templates for new anticancer agents. *Molecules.* 2015;20:3898–3941.
- Kaletsch A, Pinkerneil M, Hoffmann MJ, et al. Effects of novel HDAC inhibitors on urothelial carcinoma cells. *Clin Epigenetics.* 2018;10:1–18.
- Maolanon AR, Kristensen HME, Leman LJ, Ghadiri MR, Olsen CA. Natural and synthetic macrocyclic inhibitors of the histone deacetylase enzymes. *ChemBioChem.* 2017;18:5–49.
- Finnin MS, Donigan JR, Cohen A, et al. Structures of a histone deacetylase homologue bound to the TSA and SAHA inhibitors. *Nature.* 1999;401:188–193.
- Hai Y, Christianson DW. Histone deacetylase 6 structure and molecular basis of catalysis and inhibition. *NatChemBiol.* 2016;12:741–747.
- Krämer OH, Mahboobi S, Sellmer A. Drugging the HDAC6–HSP90 interplay in malignant cells. *Trends Pharmacol Sci.* 2014;35:501–509.
- Pan D-S, Yang Q-J, Fu X, et al. Discovery of an orally active subtype-selective HDAC inhibitor, chidamide, as an epigenetic modulator for cancer treatment. *MedChemComm.* 2014;5:1789–1796.
- Micelli C, Rastelli G. Histone deacetylases: structural determinants of inhibitor selectivity. *Drug Discov Today.* 2015;20:718–735.
- Jones PA, Issa J-PJ, Baylin S. Targeting the cancer epigenome for therapy. *Nat Rev Genet.* 2016;17:630–641.
- Zhang Y, Yan J, Yao TP. Discovery of a fluorescent probe with HDAC6 selective inhibition. *Eur J Med Chem.* 2017;141:596–602.
- Diedrich D, Hamacher A, Gertzen CGW, et al. Rational design and diversity-oriented synthesis of peptoid-based selective HDAC6 inhibitors. *Chem Commun.* 2016;52:3219–3222.
- Porter NJ, Osko JD, Diedrich D, et al. Histone deacetylase 6-selective inhibitors and the influence of capping groups on hydroxamate-zinc denticity. *J Med Chem.* 2018;61:8054–8060.
- Diedrich D, Stenzel K, Hesping E, et al. One-pot, multi-component synthesis and structure-activity relationships of peptoid-based histone deacetylase (HDAC) inhibitors targeting malaria parasites. *Eur J Med Chem.* 2018;158:801–813.
- Krieger V, Hamacher A, Gertzen CGW, et al. Design, Multicomponent synthesis, and anticancer activity of a focused histone deacetylase (HDAC) inhibitor library with peptoid-based cap groups. *J Med Chem.* 2017;60:5493–5506.
- Kong Y, Jung M, Wang K, et al. Histone deacetylase cytoplasmic trapping by a novel fluorescent HDAC inhibitor. *Mol Cancer Ther.* 2011;10:1591–1599.
- Fleming CL, Ashton TD, Nowell C, et al. A fluorescent histone deacetylase (HDAC) inhibitor for cellular imaging. *Chem Commun.* 2015;51:7827–7830.
- Ganesan A. Multitarget drugs: an epigenetic epiphany. *ChemMedChem.* 2016;1227–1241.
- de Lera AR, Ganesan A. Epigenetic polypharmacology: from combination therapy to multitargeted drugs. *Clin Epigenetics.* 2016;8:105.
- Bhatia S, Krieger V, Groll M, et al. Discovery of the first-in-class dual histone deacetylase-proteasome inhibitor. *J Med Chem.* 2018;61:10299–10309.
- Chou CJ, Herman D, Gottesfeld JM. Pimelic diphenylamide 106 is a slow, tight-binding inhibitor of class I histone deacetylases. *J Biol Chem.* 2008;283:35402–35409.
- Al-Batran SE, Homann N, Pauligk C, et al. Perioperative chemotherapy with fluorouracil plus leucovorin, oxaliplatin, and docetaxel versus fluorouracil or capecitabine plus cisplatin and epirubicin for locally advanced, resectable gastric or gastro-oesophageal junction adenocarcinoma (FLOT4): a randomised, phase 2/3 trial. *Lancet.* 2019;393:1948–1957.
- Cosconati S, Forli S, Perryman AL, Harris R, Goodsell DS, Olson AJ. Virtual screening with AutoDock: theory and practice. *Expert Opin Drug Dis.* 2010;5:597–607.
- Kalin JH, Bergman JA. Development and therapeutic implications of selective histone deacetylase 6 inhibitors. *J Med Chem.* 2013;56:6297–6313.
- Stenzel K, Hamacher A, Hansen FK, et al. Alkoxyurea-based histone deacetylase inhibitors increase cisplatin potency in chemoresistant cancer cell lines. *J Med Chem.* 2017;60:5334–5348.
- Reßing N, Marquardt V, Gertzen CGW, et al. Design, synthesis and biological evaluation of β -peptoid-capped HDAC inhibitors with anti-neuroblastoma and anti-glioblastoma activity. *MedChemComm.* 2019;10:1109–1115.
- Gediya LK, Chopra P, Purushottamachar P, Maheshwari N, Njar VCO. A new simple and high-yield synthesis of suberoylanilide hydroxamic acid and its inhibitory effect alone or in combination with retinoids on proliferation of human prostate cancer cells. *J Med Chem.* 2005;48:5047–5051.
- Mackwitz MKW, Hamacher A, Osko JD, et al. Multicomponent Synthesis and Binding Mode of Imidazo[1,2-a]pyridine-Capped Selective HDAC6 Inhibitors. *Org Lett.* 2018;20:3255–3258.
- Heltweg B, Dequiedt F, Verdin E, Jung M. Nonisotopic substrate for assaying both human zinc and NAD⁺-dependent histone deacetylases. *Anal Biochem.* 2003;319:42–48.
- Chemnitz O, Götzl K, Maurer L, et al. Response to TNF- α is increasing along with the progression in Barrett's esophagus. *Dig Dis Sci.* 2017;62:3391–3401.
- Götzl K, Chemnitz O, Maurer L, et al. In-depth characterization of the Wnt-signaling/ β -catenin pathway in an in vitro model of Barrett's sequence. *BMC Gastroenterol.* 2019;19:38.
- Shechter D, Dormann HL, Allis CD, Hake SB. Extraction, purification and analysis of histones. *Nat Protoc.* 2007;2:1445–1457.
- Schrödinger Release 2017: Maestro. Schrödinger, LLC. New York, NY. 2017.
- Muller K, Amman H, Doran D, Gerber P, Gubernator K, Schrepfer G. MOLOC: a molecular modeling program. *Bull Soc Chim Belg.* 1988;97:655–667.
- Gerber PR, Müller K. MAB, a generally applicable molecular force field for structure modelling in medicinal chemistry. *J Comput Aided Mol Des.* 1995;9:251–268.
- Millard CJ, Watson PJ, Celardo I, et al. Class I HDACs share a common mechanism of regulation by inositol phosphates. *Mol Cell.* 2013;51:57–67.
- Osterberg F, Morris GM, Sanner MF, Olson AJ, Goodsell DS. Automated docking to multiple target structures: incorporation of protein mobility and structural water heterogeneity in AutoDock. *Proteins.* 2002;46:34–40.
- Morris GM, Goodsell DS, Halliday RS, et al. Automated docking using a Lamarckian genetic algorithm and an empirical binding free energy function. *J Comput Chem.* 1998;19:1639–1662.
- Dittrich J, Schmidt D, Pflieger C, Gohlke H. Converging a knowledge-based scoring function: drugscore2018. *J Chem Inf Model.* 2019;59:509–521.